Journal of Computational and Applied Mathematics 240 (2013) 192–203

Contents lists available at SciVerse ScienceDirect

Journal of Computational and Applied Mathematics

journal homepage: www.elsevier.com/locate/cam

Upscaling for the Laplace problem using a discontinuous Galerkin method

H. Barucq [a,b], T. Chaumont Frelet [a,c], J. Diaz [a,b], V. Péron [a,b,d,*]

[a] *MAGIQUE-3D (INRIA Bordeaux – Sud-Ouest), France*

[b] *Laboratoire de Mathématiques et de leurs Applications de Pau (LMA-PAU), France*

[c] *Laboratoire Mathématique de l'INSA (LMI), France*

[d] *Université de Pau et des Pays de l'Adour, France*

ARTICLE INFO

Article history:
Received 10 February 2012
Received in revised form 7 May 2012

Keywords:
Upscaling
Laplace problem
Multiscale methods
Discontinuous Galerkin
Interior penalty

ABSTRACT

Scientists and engineers generally tackle problems that include multiscale effects and that are thus difficult to solve numerically. The main difficulty is to capture both the fine and the coarse scales to get an accurate numerical solution. Indeed, the computations are generally performed by using numerical schemes based on grids. But the stability and thus the accuracy of the numerical method depends on the size of the grid which must be refined drastically in the case of very fine scales. That implies huge computational costs and in particular the limitations of the memory capacity are often reached. It is thus necessary to use numerical methods that are able to capture the fine scale effects with computations on coarse meshes. Operator-based upscaling is one of them and we present a first attempt to adapt that technique to a Discontinuous Galerkin Method (DGM). We consider the Laplace problem as a benchmark and we compare the performance of the resulting numerical scheme with the classical one using Lagrange finite elements. The comparison involves both an accuracy analysis and a complexity calculus. This work shows that there is an interest of combining DGM with upscaling.

1. Introduction

The wave propagation is widely used in a large variety of scientific fields as in oil exploration where the issue is to produce images of hydrocarbon stocks that are hidden and nowadays very difficult to detect. The principle is based on the fact that the wave equation can be reversed in time, which means that any arrival time of a reflected wave can be transformed into a spatial measurement providing the localization of the corresponding reflector. From a numerical point of view, the process which is known as the Reverse Time Migration, requires to solve many wave equations in complex media whose tectonic includes strong heterogeneities and the contrasts of the physical parameters can thus be very significant. The quality of the image is obviously related to the accuracy of the numerical method, which justifies the development of fast and accurate solvers for large problems. The size of the discrete system is an important issue but it is not the only one. Indeed, it is necessary to consider real propagation domains, which means that multiscale problems must be solved. Propagation domains are mostly wide, while the parameters that characterize the medium vary quickly. As a consequence, the representation of the parameters should be done on a fine grid while it should be sufficient to cover the medium with a coarse mesh. Obviously, it is possible to do computations with a fine mesh whose dimensions are fixed by the physical

* Corresponding author at: Université de Pau et des Pays de l'Adour, France.
E-mail addresses: helene.barucq@inria.fr (H. Barucq), theophile.chaumont_frelet@insa-rouen.fr (T. Chaumont Frelet), julien.diaz@inria.fr (J. Diaz), victor.peron@univ-pau.fr, victor.peron@inria.fr (V. Péron).

0377-0427/$ – see front matter © 2012 Elsevier B.V. All rights reserved.
doi:10.1016/j.cam.2012.05.025

parameters. But, in that case, the resulting discrete system will contain a huge number of discrete unknowns, so that computational costs of the RTM become prohibitive, knowing that several solutions of the wave equation are needed. A numerical method capable of considering these two scales independently is thus of great interest, in particular for numerical geophysics.

To tackle multiscale problems, different attempts have been proposed in the literature. They involve upscaling, which consists in defining equivalent parameters. There exist many techniques of upscaling that are based on averaging or renormalizing the parameters [1,2]. Homogenization can also be applied [3–5]. It allows to get an accurate solution computed on the coarse grid without computing the full solution inside the fine mesh. It leads then to constant equivalent parameters. Now, it is worth noting that homogenization assumes that the parameters vary into different scales and that the medium is periodic.

In this paper, we focus on an operator-based upscaling method which can be applied without assuming periodicity of the medium. Operator-based upscaling methods were first developed for elliptic flow problems (see [6,7]) and then extended to hyperbolic problems (see [8–10]) such as the wave equation. The operator-based upscaling method is based on the splitting of the solution into two parts, the so-called rough and refined parts. The rough component is computed on a coarse grid while the refined component is obtained from computations on a fine mesh covering each coarse cell. The time computational costs can then be reduced by making calculations inside each coarse cell independent. This can be done by enforcing a Dirichlet boundary condition on the boundary of each coarse cell. By this way, the refined component is computed by solving local problems while the rough component is obtained classically by solving the variational problem inside the coarse mesh.

Operator-based upscaling methods were so far developed by using continuous finite elements. For instance, they have been carried out for wave problems by using mixed finite elements [8–10].

Herein, we consider the interest of developing an operator-based upscaling method using a Discontinuous Galerkin Finite Element Method (DGFEM). By this way, we would like to know whether it is possible to reduce the computational costs even more. DGFEMs perform well in the case of heterogeneous media because they match with hp-adaptivity and parallel computing. Nevertheless, for the same mesh, they involve more degrees of freedom than continuous FEMs. Hence, it would be interesting to see if, combined with an operator-based uspcaling, it is possible to reduce the computational costs.

This study is preliminary to a work dealing with harmonic wave equations and thus concerns the Laplace operator. We consider the standard Laplace problem with homogeneous Dirichlet boundary conditions

$$\begin{cases} -\Delta u = f & \text{in } \Omega, \\ u = 0 & \text{on } \partial\Omega, \end{cases} \tag{1}$$

where Ω is the unit square $]0,\ 1[\times]0,\ 1[$ and the source term f lies in $L^2(\Omega)$. For the sake of simplicity, we restrict ourselves to a square domain, but the study can be extended to any convex polygonal domain.

Since it is known for being both stable and consistent, we are interested in the Interior Penalty Discontinuous Galerkin Method (IPDGM) [11]. We have organized the paper in such a way that we first show how to do upscaling with an IPDGM and next we compare the performances of this approach with the one involving a continuous Finite Element Method (FEM). In Section 2, we detail the variational framework to perform upscaling with the FEM and the IPDGM. The matrices resulting from the upscaling discretization are clarified in Section 3. Section 4 is devoted to detail the upscaling algorithm and a discussion on its performances. Finally, in Section 5, we compare the performances of the algorithms using the FEM and the IPDGM through numerical results.

2. Continuous and discontinuous finite element methods for upscaling

The *upscaling* method consists in finding a finite element solution in a space $V_{H,h}$ that is decomposed into the direct sum $V_{H,h} = V_H \oplus \hat{V}_{H,h}$. The space V_H is defined on a coarse grid of characteristic length H partitioning the domain Ω, and $\hat{V}_{H,h}$ is defined on a fine grid of characteristic length h which is obtained by refining the coarse grid. Then, the approximate solution $u_{H,h}$ is obtained as $u_{H,h} = u_H + \hat{u}_{H,h}$, where $u_H \in V_H$ and $\hat{u}_{H,h} \in \hat{V}_{H,h}$. In the following, u_H is called the rough component while $\hat{u}_{H,h}$ stands for the refined component representing the small scale effects. The space $\hat{V}_{H,h}$ must be appropriately defined in such a way that $\hat{u}_{H,h}$ can be easily computed as a function of u_H. The linear system involves thus only u_H. The small scale effects are then included inside the modeling afterwards thanks to the relation between $\hat{u}_{H,h}$ and u_H.

In this section, we present two different choices for the spaces V_H and $\hat{V}_{H,h}$. The first one is adapted to continuous finite elements and has been proposed in [6,7]. The second one involves discontinuous finite elements which we would like to focus on. Herein, we consider the IPDGM. Once the spaces are introduced, we define the corresponding bilinear forms.

2.1. Definition of the finite element spaces

Before introducing the finite element spaces, we need to define a partition of the domain Ω. For the sake of simplicity, we restrict ourselves to regular Cartesian meshes in two dimensions, but our study can be extended without difficulty to irregular meshes or to three dimensional problems. We fix $N, M \in \mathbb{N}^*$, and we define two mesh sizes $H = 1/N$ (the coarse

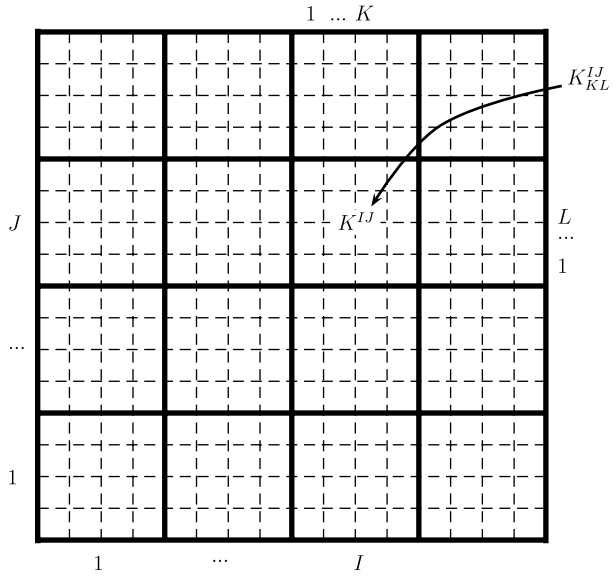

Fig. 1. The mesh $\mathcal{T}_H$ (solid lines) and the submesh $\mathcal{T}_h$ (dashed lines).

step), and $h = H/M$ (the fine step). The coordinates of the coarse nodes are defined by $X^I = IH$ (for $0 \leq I \leq N$) and $Y^J = JH$ (for $0 \leq J \leq N$). Then, we define the coarse cells K^{IJ} and the coarse mesh $\mathcal{T}_H$ by

$$K^{IJ} =]X^{I-1}, X^I[\times]Y^{J-1}, Y^J[\quad (1 \leq I, J \leq N), \qquad \mathcal{T}_H = \left\{K^{IJ}\right\}_{I,J=1}^{N}.$$

We subdivide each coarse cell K^{IJ} with fine cells. We define $X_P^I = X^I + Ph$ (for $0 \leq P \leq M$) and $Y_Q^J = Y^J + Qh$ (for $0 \leq Q \leq M$). We then define the fine cells K_{PQ}^{IJ} by

$$K_{PQ}^{IJ} =]X_{P-1}^{I-1}, X_P^{I-1}[\times]Y_{Q-1}^{J-1}, Y_Q^{J-1}[,$$

which defines the submesh $\mathcal{T}_{H,h}^{IJ} = \left\{K_{PQ}^{IJ}\right\}_{P,Q=1}^{M}$ and the global fine mesh, which is the union of all submeshes:

$$\mathcal{T}_h = \bigcup_{I,J=1}^{N} \mathcal{T}_{H,h}^{IJ}. \tag{2}$$

In Fig. 1, we represent the mesh $\mathcal{T}_H$ and its submesh $\mathcal{T}_h$.

The set of internal edges of $\mathcal{T}_h$ is denoted by $\mathcal{F}_h^i$ with

$$\mathcal{F}_h^i = \left\{e = \partial K \cap \partial J \mid K, J \in \mathcal{T}_h\right\},$$

while the set of external edges of $\mathcal{T}_h$ is

$$\mathcal{F}_h^b = \left\{e = \partial K \cap \partial \Omega \mid K \in \mathcal{T}_h\right\}.$$

The set of all edges of $\mathcal{T}_h$ is thus

$$\mathcal{F}_h = \mathcal{F}_h^i \cup \mathcal{F}_h^b. \tag{3}$$

Now, we introduce the usual discretization spaces V_H and V_h involved in the FEM we apply. Here, we use the same notations for continuous FEMs and for IPDGMs. Regarding the FEM, the discretization space V_H on the coarse grid, called "rough discretization space", is defined by

$$V_H = \left\{v \in C^0(\bar{\Omega}) \mid \forall K \in \mathcal{T}_H \ v|_K \in \mathbb{Q}_p(K), \text{ and } v|_{\partial\Omega} = 0\right\},$$

where $\mathbb{Q}_p(K), p \in \mathbb{N}$ is the space of polynomials of degree at most p in each variable on the element K. Concerning the IPDGM, V_H is defined by

$$V_H = \left\{v \in L^2(\Omega) \mid \forall K \in \mathcal{T}_H, \ v|_K \in \mathbb{Q}_p(K)\right\}.$$

It should be noted that the main difference between the two spaces lies in the fact that the solution to discontinuous Galerkin problem is only piecewise continuous. Therefore, it is not in $C^0(\bar{\Omega})$ but only in $L^2(\Omega)$.

Let us introduce V_h, which is built on the full fine grid $\mathcal{T}_h$ and is defined by

$$V_h = \left\{ v \in C^0(\bar{\Omega}) \mid v|_K \in \mathbb{Q}_p(K),\ \forall K \in \mathcal{T}_h \right\},$$

for the FEM and as

$$V_h = \left\{ v \in L^2(\Omega) \mid v|_K \in \mathbb{Q}_p(K),\ \forall K \in \mathcal{T}_h \right\},$$

for the IPDGM.

Let us now remark that, since $\mathcal{T}_h$ is constructed as a refinement of $\mathcal{T}_H$, $V_H \subset V_h$ and the sum of the two spaces is not direct. Then, we introduce a third vector space, $\hat{V}_{H,h}$, which is specific to the *upscaling* method. This space $\hat{V}_{H,h}$ is associated with both meshes $\mathcal{T}_H$ and $\mathcal{T}_h$, and is defined for both continuous and discontinuous approximations by

$$\hat{V}_{H,h} = \left\{ v \in V_h \mid \forall K \in \mathcal{T}_H \quad v|_{\partial K} = 0 \right\}. \tag{4}$$

Then, it is clear that the sum of V_H and $\hat{V}_{H,h}$ is direct, provided that $p < N^2 + 1$, and we can define the upscaling discretization space

$$V_{H,h} = V_H \oplus \hat{V}_{H,h}.$$

Note that $V_H \subset V_{H,h} \subset V_h$. The condition $v|_{\partial K} = 0$ in (4) is crucial for the upscaling method, since it allows for a simple calculation of the refined part $\hat{u}_{H,h}$ of the solution from the knowledge of the rough part u_H. We will detail this property in the next section. The condition $p < N^2 + 1$ ensures that no element of V_H could satisfy the condition $v|_{\partial K} = 0$ on all edges of the coarse mesh. It is always satisfied for practical applications, since p is generally smaller than 10 and N greater than 10.

To describe more precisely the upscaling algorithm, we also need to define the spaces $\hat{V}^{IJ}_{H,h}$, whose elements v are the restrictions of $v \in \hat{V}_{H,h}$ on a coarse cell $K^{IJ} \in \mathcal{T}_H$,

$$\hat{V}^{IJ}_{H,h} = \left\{ v \in \hat{V}_{H,h} \mid \text{Supp } v \subset K^{IJ} \right\},$$

and the spaces V^{IJ}_H whose elements v are the restrictions of $v \in V_H$ on $K^{IJ} \in \mathcal{T}_H$,

$$V^{IJ}_H = \left\{ v \in V_H \mid \text{Supp } v \subset K^{IJ} \right\}.$$

Then, there holds $\hat{V}_{H,h} = \bigoplus_{I,J=1}^{N} \hat{V}^{IJ}_{H,h}$, $\quad V_H = \bigoplus_{I,J=1}^{N} V^{IJ}_H$.

Now, let us focus on the bilinear form associated to the upscaling problem.

2.2. Bilinear forms associated with continuous and discontinuous finite element methods

The discretized problem reads: find $u_{H,h} \in V_{H,h}$ such that, $\forall v \in V_{H,h}$,

$$a_h(u_{H,h}, v) = \int_\Omega f\ v\, dx, \tag{5}$$

where a_h is a bilinear form, coercive on $V_{H,h}$. In the case of continuous finite elements, we have

$$a_h(u, v) = \int_\Omega \nabla u \cdot \nabla v\, dx.$$

For discontinuous finite element methods there are many kinds of Discontinuous Galerkin formulations, each of them leading to a different definition of a_h. We refer to [11] for a review of these formulations and a detailed study of their stability and convergence properties. Herein, we have chosen to focus on an IPDGM, which has been proposed by Arnold in [12] and is also known as Symmetric Interior Penalty method [13]. It has been shown in [11] that this method is stable and consistent, which means that the convergence order is optimal, contrary to many other DGFEMs. This is the reason why we have chosen to favor IPDGMs, but the upscaling method can be applied to any other type of DGFEMs without difficulty.

We first need to define the notion of "jump" and "mean" of a discontinuous function through an edge. Let e be an internal edge shared by two elements denoted arbitrarily by K and J: $e = \partial K \cap \partial J \in \mathcal{F}^i_h$. We denote by n_K the unit normal vector to e (see Fig. 2), outward to K, and we define the jump of a scalar function $u \in V_h$ and the mean of a vector function $v \in V^2_h$ through e by

$$[[u]]_e = u_K|_e - u_J|_e, \qquad \{\{v\}\}_e = \frac{v_K|_e + v_J|_e}{2} \cdot n_K.$$

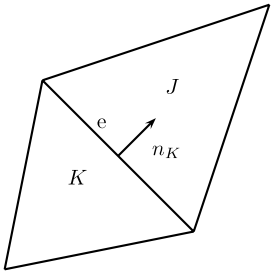

Fig. 2. The elements K and J and the normal vector n_K.

For an external edge $e = \partial K \cap \partial\Omega \in \mathcal{F}_h^b$, the jump of u and the mean value of v are defined by analogy as

$$[[u]]_e = u|_e, \qquad \{\{v\}\}_e = v|_e \cdot n_K.$$

The interior penalty bilinear form a_h is defined for all $u, v \in V_{H,h}$ by

$$a_h(u, v) = B_h(u, v) - I_h(u, v) - I_h(v, u) + J_h(u, v), \tag{6}$$

where

$$B_h(u, v) = \sum_{K\in\mathcal{T}_h} \int_K \nabla u \cdot \nabla v dx,$$

$$I_h(u, v) = \sum_{e\in\mathcal{F}_h} \int_e [[u]]\{\{\nabla v\}\} ds,$$

$$J_h(u, v) = \sum_{e\in\mathcal{F}_h} \int_e \frac{\alpha}{h} [[u]][[v]] ds,$$

and α is a constant (independent of H and h) that can be chosen large enough to make a_h coercive (see [14,15]) on the space V_h. We define the norm $\| \|_{DG}$ by [16]

$$\|u\|_{DG}^2 = \sum_{K\in\mathcal{T}_h} \|\nabla u\|_{0,K}^2 + \sum_{e\in\mathcal{F}_h} h^{-1} \|[[u]]\|_{0,e}^2.$$

Here, we denote by $\| \cdot \|_{0,K}$ the norm in $L^2(K)$, and by $\| \cdot \|_{0,e}$ the norm in $L^2(e)$. Recall that $\mathcal{T}_h$ is the global fine mesh (2), and $\mathcal{F}_h$ is the set of all edges of $\mathcal{T}_h$ (3).

According to the definition of $V_{H,h}$, this norm is equivalent on the spaces $V_{H,h}$ and V_h. Hence, since a_h is coercive on V_h, a_h is coercive on $V_{H,h}$ and the problem (5) has a unique solution $u_{H,h} \in V_{H,h}$.

2.3. Upscaling formulation

We seek a discrete solution under the form $u_{H,h} = u_H + \hat{u}_{H,h}$ in $V_{H,h}$, where $u_H \in V_H$ and $\hat{u}_{H,h} \in \hat{V}_{H,h}$. The unknown $u_{H,h}$ is solution to the discrete problem

$$a_h(u_{H,h}, v_{H,h}) = L(v_{H,h}) \quad \forall v_{H,h} \in V_{H,h}.$$

Using the direct decomposition of $V_{H,h} = V_H \oplus \hat{V}_{H,h}$, we obtain the system of variational equations

$$\begin{cases} a_h(u_H + \hat{u}_{H,h}, v_H) = L(v_H) & \forall v_H \in V_H \\ a_h(u_H + \hat{u}_{H,h}, \hat{v}_{H,h}) = L(\hat{v}_{H,h}) & \forall \hat{v}_{H,h} \in \hat{V}_{H,h}. \end{cases} \tag{7}$$

Thanks to the direct sum $\hat{V}_{H,h} = \bigoplus_{I,J=1}^N \hat{V}_{H,h}^{IJ}$, the second equation is then transformed into a collection of subproblems for $1 \le I, J \le N$. Indeed, using that

$$\hat{u}_{H,h} = \sum_{I,J=1}^N \hat{u}_{H,h}^{IJ},$$

each $\hat{u}_{H,h}^{IJ}$ satisfies the problem

$$a_h(\hat{u}_{H,h}^{IJ}, \hat{v}_{H,h}^{IJ}) = L(\hat{v}_{H,h}^{IJ}) - a_h(u_H, \hat{v}_{H,h}^{IJ}) \quad \forall \hat{v}_{H,h}^{IJ} \in \hat{V}_{H,h}^{IJ}. \tag{8}$$

Observe now that in (8), u_H get involved in the right-hand side and we do not know its value at this stage. However, thanks to the homogeneous Dirichlet boundary condition on ∂K^{IJ} which is imposed in the space $V_{H,h}^{IJ}$, we can assume that each subproblem is independent and well-posed on K^{IJ} when u_H is a data. Thus, we can use each subproblem to obtain the expression $\hat{u}_{H,h}^{IJ}(u_H)$ as a function of u_H. Assembling all the solutions, we then obtain a way of computing $\hat{u}_{H,h}$ as a function of u_H. At this point, we are able to insert this expression in the first equation of (7) to get the variational equation

$$a_h(u_H + \hat{u}_{H,h}(u_H), v_H) = L(v_H) \quad \forall v_H \in V_H, \tag{9}$$

whose only unknown is u_H.

The upscaling algorithm we use is then the following. As a first step, by solving the subproblems (8) we find the expression of $\hat{u}_{H,h}$ which depends on u_H. The second step consists in solving the rough equation (9) in order to compute u_H. The final step consists in computing $u_{H,h}$ from u_H thanks to the expression we obtained at step 1.

The main advantage of this algorithm is that there is no need to compute the solution on the whole fine grid covering Ω. We just have to solve subproblems defined on a fine scale, but on small subparts of Ω (the coarse cells K^{ij}) plus a problem on the whole domain, but defined on a coarse scale.

3. Properties of the linear systems

In order to describe the shape of the stiffness matrix $\mathcal{K}$ resulting from the upscaling discretization, we have to introduce a basis of $V_{H,h}$. This basis is obtained from basis of V_H and $\hat{V}_{H,h}$.

We denote by $(\psi_i)_{i=1..N_H}$ a basis of V_H, N_H being the number of degrees of freedom of the mesh $\mathcal{T}_H$. By construction of $\hat{V}_{H,h}$, it is represented by the set $\left(\phi_k^{IJ}\right)_{k=1..M_h}$ of basis functions related to $\hat{V}_{H,h}^{IJ}$ for $(I,J) \in 1 \ldots N^2$. Here M_h denotes the number of degrees of freedom of the submesh of K^{IJ}. We will consider classical Lagrange basis functions, but using other types of basis functions should not impact on the properties of the resulting matrix. Concerning the global numbering of the nodes of the fine mesh, we choose, without loss of generality, to number them coarse cells by coarse cells, from bottom to top and from left to right.

The matrix $\mathcal{K}$ is then constructed as the assembling of four blocks. The first one, denoted by $\mathcal{K}_{cc}$, corresponds to the interactions between the basis functions of V_H. The second one, denoted by $\mathcal{K}_{ff}$, corresponds to the interactions between the basis functions of $\hat{V}_{H,h}$. The two last ones, denoted by $\mathcal{K}_{cf}$ and $\mathcal{K}_{fc}$, correspond to the interactions between the basis functions of V_H and the basis functions of $\hat{V}_{H,h}$. Since the bilinear form a_h is symmetric, we have $\mathcal{K}_{cf} = \mathcal{K}_{fc}^{\mathrm{T}}$.

- The coarse matrix $\mathcal{K}_{cc}$ is defined by

  $$(\mathcal{K}_{cc})_{i,j} = a_h(\psi_i, \psi_j), \quad 1 \le i, j \le N_H.$$

  It corresponds to the standard stiffness matrix we would obtain by using a standard FEM applied on the coarse mesh only. It is thus symmetric positive definite.
- To define the fine matrix $\mathcal{K}_{ff}$, we first introduce the elementary "fine stiffness matrix" associated with the coarse cell $K^{IJ} \in \mathcal{T}_H$:

  $$\left(\mathcal{K}_{ff}^{IJ}\right)_{i,j} = a_h(\phi_i^{IJ}, \phi_j^{IJ}), \quad 1 \le i, j \le M_h.$$

  To construct the fine matrix $\mathcal{K}_{ff}$ we use the following proposition.

Property 1. *The matrix $\mathcal{K}_{ff}$ is block diagonal and each block is an elementary matrix $\mathcal{K}_{ff}^{IJ}$.*

This property follows from the choice of the space $\hat{V}_{H,h}^{IJ}$ and in particular from the condition $v_{|\partial K} = 0$ on the boundary of each coarse cell.

Proof. We just have to prove that the bilinear form $a_h(\phi_i^{IJ}, \phi_j^{PQ})$ vanishes as soon as $(I,J) \neq (P,Q)$ (i.e. when we consider the interactions between two distinct elements K^{IJ} and K^{PQ}).

The result is obvious for the FEM. Indeed, two functions ϕ_i^{IJ} and ϕ_j^{PQ} with $(I,J) \neq (P,Q)$ have separated supports since we impose a Dirichlet condition on the boundary of each coarse cell. Hence we have $a_h(\phi_i^{IJ}, \phi_j^{PQ}) = 0$. We therefore focus on the IPDGM case.

If K^{IJ} and K^{PQ} share no common edges, it is clear that $a_h(\phi_i^{IJ}, \phi_j^{PQ}) = 0$. If they share a common edge e, we have

$$B_h(\phi_i^{IJ}, \phi_j^{PQ}) = 0,$$

$$J_h(\phi_i^{IJ}, \phi_j^{PQ}) = \int_e [[\phi_i^{IJ}]][[\phi_j^{PQ}]]ds,$$

$$I_h(\phi_j^{PQ}, \phi_i^{IJ}) = \int_e [[\phi_j^{PQ}]]\{\{\nabla\phi_i^{IJ}\}\}ds,$$

$$I_h(\phi_i^{IJ}, \phi_j^{PQ}) = \int_e [[\phi_i^{IJ}]]\{\{\nabla\phi_j^{PQ}\}\}ds.$$

Since e is an edge of the coarse elements K^{IJ} and K^{PQ}, we have $[[\phi_i^{IJ}]]_e = [[\phi_j^{PQ}]]_e = 0$, thanks to the Dirichlet boundary condition imposed on the boundary of the coarse cell. Then, we have

$$J_h(\phi_i^{IJ}, \phi_j^{PQ}) = I_h(\phi_i^{IJ}, \phi_j^{PQ}) = I_h(\phi_j^{PQ}, \phi_i^{IJ}) = 0.$$

We conclude that $\mathcal{K}_{ff}$ is block diagonal and its diagonal blocks are $\mathcal{K}_{ff}^{IJ}$. □

We then obtain the full "fine matrix" by assembling each block:

$$\mathcal{K}_{ff} = \left\{\mathcal{K}_{ff}^{IJ}\right\} \quad 1 \le I \le N,\ 1 \le J \le N.$$

Moreover, from the properties of the bilinear form a_h, we easily check that each block is symmetric positive definite and thus invertible.

Remark 1. In the case of regular Cartesian meshes of homogeneous domains, the matrix $\mathcal{K}_{ff}^{IJ}$ is the same for each coarse cell.

- We use a similar process to define the matrix $\mathcal{K}_{cf}$. For each cell $K^{IJ} \in \mathcal{T}_H$, we define the submatrix $\mathcal{K}_{cf}^{IJ}$

$$(\mathcal{K}_{cf}^{IJ})_{k,l} = \left\{a_h(\psi_k, \phi_l^{IJ})\right\}, \quad 1 \le k \le N_H,\ 1 \le I, J \le N,\ 1 \le l \le M_h,$$

and we set

$$\mathcal{K}_{cf} = \left\{\mathcal{K}_{cf}^{IJ}\right\} \quad 1 \le I \le N,\ 1 \le J \le N.$$

Note that $(\mathcal{K}_{cf}^{IJ})_{k,l}$ obviously vanishes if the support of the coarse basis function ψ_k does not contain the element K^{IJ}.

We can now define the "full upscaled matrix" $\mathcal{K}$ (associated with the upscaling space $V_{H,h}$) by assembling the different blocks:

$$\mathcal{K} = \begin{pmatrix} \mathcal{K}_{cc} & \mathcal{K}_{cf} \\ \mathcal{K}_{cf}^{\mathrm{T}} & \mathcal{K}_{ff} \end{pmatrix}. \tag{10}$$

4. Upscaling algorithm

In this section, we first detail the upscaling algorithm to solve the Laplace problem (5) in the space $V_{H,h} = V_H \oplus \hat{V}_{H,h}$, using the expression of the stiffness matrix $\mathcal{K}$. Then, we discuss the performance of the method.

4.1. Upscaling for solving the Laplace problem

In the following, we denote by U_H the vector of size N_H representing the decomposition of the rough solution u_H in the basis $(\psi_i)_{i=1..N_H}$ and by $\hat{U}_{H,h}$ the vector of size $N^2 * M_h$ representing the decomposition of the refined solution $\hat{u}_{H,h}$ in the basis $\left(\phi_k^{IJ}\right)_{\substack{k=1..M_h \\ I,J=1..N}}$. The vector $U_{H,h} = (U_H, \hat{U}_{H,h})^{\mathrm{T}}$ corresponds then to the total solution $u_{H,h}$. We use a similar decomposition to compute the source term $F = (F_c, F_f)^{\mathrm{T}}$. Here,

$$F_c = \{(f, \psi_i)\}_{i=1..N_H},$$
$$F_f = \{(f, \phi_k^{IJ})\}_{\substack{k=1..M_h \\ I,J=1..N}}.$$

Then, the matricial form of the discretized Laplace problem reads

$$\mathcal{K} U_{H,h} = F.$$

Hence, using the decomposition (10) of the stiffness matrix $\mathcal{K}$, we are led to solve the block linear system

$$\begin{pmatrix} \mathcal{K}_{cc} & \mathcal{K}_{cf} \\ \mathcal{K}_{cf}^{\mathrm{T}} & \mathcal{K}_{ff} \end{pmatrix} \begin{pmatrix} U_H \\ \hat{U}_{H,h} \end{pmatrix} = \begin{pmatrix} F_c \\ F_f \end{pmatrix}.$$

Now, we express $\hat{U}_{H,h}(U_H)$ as a function of U_H:

$$\hat{U}_{H,h} = \mathcal{K}_{ff}^{-1} F_f - \mathcal{K}_{ff}^{-1} \mathcal{K}_{cf}^{\mathrm{T}} U_H, \tag{11}$$

and we obtain a linear system where the only unknown is the rough solution U_H:

$$(\mathcal{K}_{cc} - \mathcal{K}_{cf} \mathcal{K}_{ff}^{-1} \mathcal{K}_{cf}^{\mathrm{T}}) U_H = F_c - \mathcal{K}_{cf} \mathcal{K}_{ff}^{-1} F_f. \tag{12}$$

Since the matrix $\mathcal{K}_{ff}$ is block diagonal (as proved in the previous section), inverting $\mathcal{K}_{ff}$ resumes to invert each $\mathcal{K}_{ff}^{IJ}$. We thus discern the three steps of the algorithm:

1. Solving the subproblems in order to obtain the expression (11) of $\hat{U}_{H,h}$ in terms of U_H. This step resumes to invert the submatrices $\mathcal{K}_{ff}^{II}$.
2. Solving the coarse equation (12) to get U_H.
3. Using the value of U_H previously computed in (11) in order to get $\hat{U}_{H,h}$.

Note that it is not necessary to invert the total matrix $\mathcal{K}$. We just have to invert the matrices $\mathcal{K}_{ff}^{II}$ (which correspond to fine-scale problems on subparts of Ω) and $\mathcal{K}_{cc}$ (which corresponds to a coarse-scale problem on Ω).

4.2. Performance of the method

We discuss here the performance of the algorithm. We can easily give an asymptotic cost of the method if we consider that most part of computations consists in inverting matrices. We assume that inverting an $l \times l$ matrix requires $\mathcal{O}(l^3)$ operations.

We introduce γ_p as the number of degree of freedom per cell. There holds $\gamma_p = (p+1)^2$ for the IPDGM and $\gamma_p = 4/4 + 4(p-1)/2 + (p-1)^2 = p^2$ for the continuous FEM (four nodes shared by four elements, $p-1$ nodes shared by two elements on each edge and $(p-1)^2$ internal elements).

The algorithm requires to invert each square matrix $\mathcal{K}_{ff}^{ii}$. There are N^2 matrices $\mathcal{K}_{ff}^{ii}$ and the size of each one is $\gamma_p M^2$. Therefore, solving the subproblems requires $\mathcal{O}(\gamma_p^3 N^2 M^6)$ operations. To solve the coarse-scale equations, we need to invert the matrix $\mathcal{K}_{cc} - \mathcal{K}_{cf}\mathcal{K}_{ff}^{-1}\mathcal{K}_{cf}^{\mathrm{T}}$ which is of size $\gamma_p N^2$. Thus, solving the coarse problem represents $\mathcal{O}(\gamma_p^3 N^6)$ operations. The asymptotic cost of the algorithm is thus of order $(N^2M^6 + N^6)\gamma_p^3$.

We can now compare this result with the standard IPDGM and FEM (without upscaling) on the coarse grid only and on the full fine grid. In the coarse grid, we need to invert $\mathcal{K}_{cc}$, therefore the asymptotic cost is $\mathcal{O}(N^6\gamma_p^3)$ operations. In the full fine grid, we need to invert a matrix of size $\gamma_p N^2 M^2$. Hence, the asymptotic cost is $\mathcal{O}(N^6M^6\gamma_p^3)$.

To conclude, when studying a very heterogeneous domain ($M \gg N$) the upscaling algorithm is approximately N^4 times less expensive than solving the full fine scale problem.

5. Numerical experiments

We now present numerical experiments devoted to analyze and to compare the performance of the upscaling algorithm using the FEM and the IPDGM. We carry out two tests in a 2D square domain of size $\Omega = 1\mathrm{m} \times 1\mathrm{m}$. In the first test, we consider a source function with slow variations. This test is similar to the one presented in [10] and illustrates how the approximated solution converges when the space steps H and h decrease. Then we consider a source function which presents much more oscillations. This test case illustrates more precisely the advantages of using an upscaling algorithm instead of considering the classical FEM or IPDGM. The two source functions are chosen such that the analytic solution u of the Laplace problem can be easily computed. Then, we can calculate the "rough" L^2-error E^r, between u and the rough solution u_H and the "total" L^2-error E^t between u and the total solution $u_{H,h}$ as

$$E^r = \|u - u_H\|_0 \quad \text{and} \quad E^t = \|u - u_{H,h}\|_0.$$

In all tests, we use $\mathbb{Q}_1$ finite elements. Now, we recall the classical convergence properties of the FEM and the IPDGM. When using the usual discretization space V_H, the IPDGM with $\mathbb{Q}_p$ elements converges like H^{p+1} in the L^2 norm for the Laplace problem; see [15,11]. Therefore, we expect to observe a space-convergence of second order when we refine the coarse mesh $\mathcal{T}_H$. Concerning the standard FEM, it is well known that the method converges like H^{p+1}, when using the usual discretization space V_H. We therefore expect once again a second order convergence.

5.1. The case of a slowly oscillating function

Relying on several numerical tests performed in [10], we consider a source function $f(x,y) = \sin(\pi x)\sin(\pi y)$. This function was chosen in order to produce the solution

$$u(x,y) = \frac{1}{2\pi^2}\sin(\pi x)\sin(\pi y).$$

First, we fix the number of fine cells M in each coarse cell and we refine the coarse mesh. This test enables us to show that the upscaling algorithm "preserves" the original convergence properties of the IPDGM and the FEM. Then, we investigate the properties of the algorithm when the fine mesh only is refined. We fix the number of coarse cells N and we increase the number of fine cells in each coarse cell.

We thus first consider a $N \times N$ coarse mesh, where N ranges from 10 to 50. We refine each coarse cell with a fixed number of 5×5 cells. The "rough errors" and "total errors" are presented in Table 1 and the graphs are plotted in Fig. 3. We observe a second order convergence for both the rough solution and the total solution and for both IPDGM and FEM, which is the result we expected. There is no major difference between the accuracy of the two methods.

Table 1
Errors E^r and E^t as functions of H and h.

H	h	IPDGM		FEM	
		E^r	E^t	E^r	E^t
0.1000	0.0200	2.46×10^{-4}	6.54×10^{-5}	2.08×10^{-4}	6.36×10^{-5}
0.0500	0.0100	6.16×10^{-5}	1.59×10^{-5}	5.20×10^{-5}	1.57×10^{-5}
0.0333	0.0067	2.73×10^{-5}	7.03×10^{-6}	2.31×10^{-5}	6.96×10^{-6}
0.0250	0.0050	1.54×10^{-5}	3.94×10^{-6}	1.30×10^{-5}	3.91×10^{-6}
0.0200	0.0040	9.85×10^{-6}	2.52×10^{-6}	8.33×10^{-6}	2.50×10^{-6}

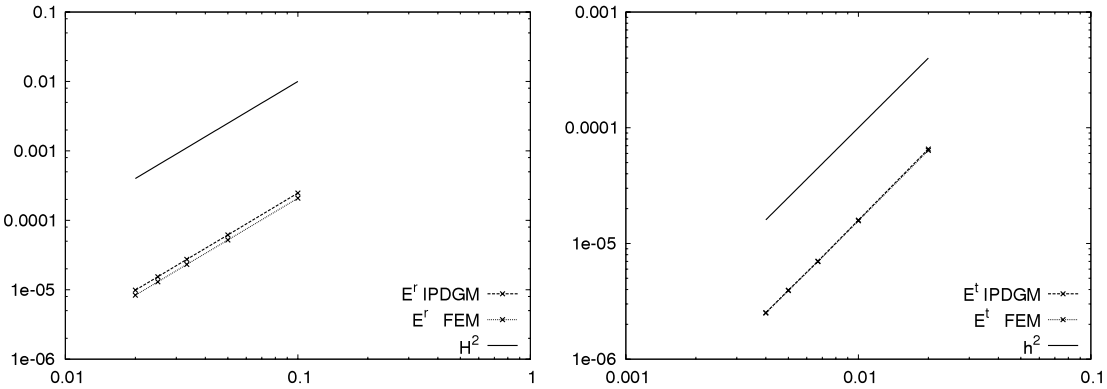

Fig. 3. Errors E^r and E^t as functions of H and h.

Table 2
Errors E^r and E^t as functions of h. $H = 0.2$.

h	IPDGM		FEM	
	E^r	E^t	E^r	E^t
0.0667	9.84×10^{-4}	3.61×10^{-4}	8.35×10^{-4}	3.50×10^{-4}
0.0333	9.92×10^{-4}	2.79×10^{-4}	8.35×10^{-4}	2.57×10^{-4}
0.0167	9.93×10^{-4}	2.64×10^{-4}	8.35×10^{-4}	2.41×10^{-4}
0.00833	9.93×10^{-4}	2.61×10^{-4}	8.35×10^{-4}	2.37×10^{-4}

Now, we fix the coarse grid to 5×5 cells and we divide the fine grid step by 2 in each subtest (hence M ranges from 3 to 24). The results are presented in Table 2. We observe that the error on the rough solution remains approximately constant. It is not surprising since the coarse mesh remains unchanged. Actually the rough error obtained by an FEM is totally independent of the fine mesh. This is due to the fact that, in the very particular case of $\mathbb{Q}_1$-Lagrange elements with regular meshes in homogeneous media, the matrix $\mathcal{K}_{cf}$ is null. This can be proved by a direct but tedious calculation of $a_h(\psi_k, \phi_l^{ij})$.

Concerning the total solution, we observe that accuracy is improved when the fine mesh is refined. Yet, this accuracy is less and less significant as h decreases. This result confirms the observation of [10], where the authors have shown that there is no second order convergence when only the fine mesh is refined.

5.2. The case of a more rapidly oscillating function

In the next experiment, we chose a source term f ($f(x, y) = 2\pi^2[\sin(\pi x)\sin(\pi y) + 8.1\sin(9\pi x)\sin(9\pi y)]$) which produces the following solution

$$u(x, y) = \sin(\pi x)\sin(\pi y) + 0.1\sin(9\pi x)\sin(9\pi y).$$

This solution is composed of two parts. The first one oscillates slowly with a large amplitude, while the second part oscillates rapidly with a lower amplitude. This experiment is devoted to mimic physical problems where the properties of the media vary rapidly but with a small amplitude around a mean smooth function.

Hereafter, we consider three test-cases.

(a) We fix the number of fine cells in each coarse cell to 5×5. We refine a $N \times N$ coarse mesh, where N ranges from 5 to 50. The numerical values of the errors are presented in Table 3. As shown in the previous experiment, we observe again a second order convergence for both the rough solution and the total solution. Once again, there is no major difference between the IPDGM and the FEM.

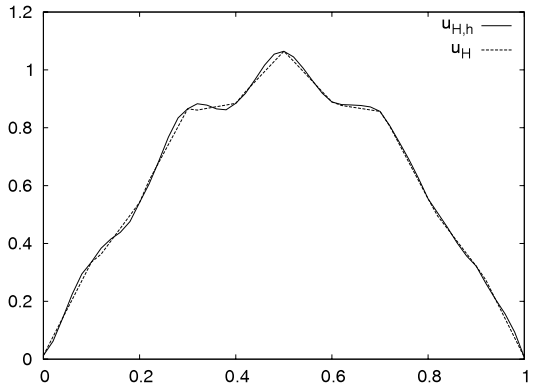

Fig. 4. Rough solution u_H, and total solution $u_{H,h}$ obtained with IPDGM. $H = 0.1$, $h = 0.02$, $y = 0.48$.

Table 3
Errors E^r and E^t as functions of H and h.

H	h	IPDGM		FEM	
		E^r	E^t	E^r	E^t
0.2000	0.0400	3.69×10^{-1}	3.97×10^{-1}	3.71×10^{-1}	3.91×10^{-1}
0.1000	0.0200	3.50×10^{-2}	2.62×10^{-2}	7.37×10^{-3}	2.26×10^{-2}
0.0500	0.0100	1.01×10^{-2}	4.18×10^{-3}	8.24×10^{-3}	3.47×10^{-3}
0.0333	0.0067	4.46×10^{-3}	1.48×10^{-3}	3.73×10^{-3}	1.31×10^{-3}
0.0250	0.0050	2.50×10^{-3}	7.51×10^{-4}	2.10×10^{-3}	6.88×10^{-4}
0.0200	0.0040	1.60×10^{-3}	4.54×10^{-4}	1.35×10^{-3}	4.27×10^{-4}

Table 4
Errors E^r and E^t as functions of h.

H	h	IPDGM		FEM	
		E^r	E^t	E^r	E^t
0.0500	0.0167	9.80×10^{-3}	4.42×10^{-3}	8.24×10^{-3}	4.19×10^{-3}
0.0500	0.0083	1.01×10^{-2}	4.42×10^{-3}	8.24×10^{-3}	3.37×10^{-3}
0.0500	0.0042	1.02×10^{-2}	4.41×10^{-3}	8.24×10^{-3}	3.23×10^{-3}
0.0500	0.0021	1.02×10^{-2}	4.41×10^{-3}	8.24×10^{-3}	3.20×10^{-3}

Table 5
Errors E_H as function of H.

H	FEM	IPDGM
0.2000	3.71×10^{-1}	1.87
0.1000	7.37×10^{-3}	1.20×10^{-1}
0.0500	8.24×10^{-3}	4.07×10^{-2}
0.0333	3.73×10^{-3}	2.00×10^{-2}
0.0250	2.10×10^{-3}	1.17×10^{-2}
0.0200	1.35×10^{-3}	7.64×10^{-3}
0.0100	3.36×10^{-4}	1.97×10^{-3}
0.0050	8.39×10^{-4}	4.95×10^{-4}

(b) In the second test, we fix the rough step size to 0.05 and we reduce the fine grid step of 2 in each subtest. The rough part u_H, and the total solution $u_{H,h}$ obtained by the IPDGM for $H = 0.1$, $h = 0.02$, and $y = 0.48$ are displayed in Fig. 4.
As observed in the previous experiment (see Section 5.1), we see from Table 4 that the errors are again approximately constants. Therefore, if the coarse mesh is not refined the convergence cannot be expected. Once again, there is no variation of the rough error for the FEM, due to the fact that the matrix $\mathcal{K}_{cf}$ is null.

(c) In the last experiment, we compute the L^2 errors E_H between the analytic solution u and the approximated solution u_H obtained by the two methods (the FEM and the IPDGM) without upscaling. The results are presented in Table 5. Before computing the error, we have projected the approximated solution on a refined grid of space step $h = H/5$, in order to obtain accurate results.
In comparison with standard FEM and IPDGM, we observe that the upscaling method improves the accuracy of the augmented solution. Compare for instance line $H = 0.05$ in Table 5 with line $H = 0.05, h = 0.01$ in Table 3. The improvement is more significant for IPDGMs, where the total error is ten times smaller than the error obtained with

Table 6
Computational time for upscaling with FEM.

H	h	CPU time
0.2000	0.0400	0.008
0.1000	0.0200	0.020
0.0500	0.0100	0.076
0.0333	0.0067	0.212
0.0250	0.0050	0.580
0.0200	0.0040	1.540

Table 7
Computational time for classical FEM.

H	CPU time
0.2000	0.000
0.1000	0.004
0.0500	0.020
0.0333	0.100
0.0250	0.384
0.0200	1.220
0.0100	68.60
0.0050	4380

standard IPDGMs. As it was expected, we note that classical FEMs and IPDGMs are more accurate on the fine mesh than upscaling (compare for instance line $H = 0.01$ in Table 5 with line $H = 0.05$, $h = 0.01$ in Table 3).

In order to emphasize the gain we obtain using an upscaling technique, we present respectively in Tables 6 and 7 the computational time of upscaling with the FEM and of the classical FEM. Comparing line $H = 0.1$, $h = 0.02$ in Table 6 with lines $H = 0.1$ and $H = 0.02$ in Table 7, we observe that the computational cost of the upscaling technique is five times greater than the cost of the classical technique on a coarse grid but 60 times smaller than the cost of the classical technique on a fine grid. The gain is increased when we refine the grid: for $H = 0.05$, $h = 0.01$, the computational cost of the upscaling technique is four times greater than the cost of the classical technique on a coarse grid but 1000 times smaller than the cost of the classical technique on a fine grid. Finally, for $H = 0.025$, $h = 0.005$, the upscaling technique is only 1.5 times more expensive than the classical technique on a coarse grid, while it is 7500 cheaper than the classical technique on a fine grid.

6. Conclusion

Operator-based uspcaling allows numerical computations on very fine meshes to be sidestepped and thus contributes well to reduce the computational costs of finite element methods. It is based on the idea of solving subproblems covered by a fine grid after the computational domain being divided into independent subdomains.

By considering the Laplace problem, we have carried out operator-based uspcaling when using continuous and discontinuous Galerkin finite elements. The combination of upscaling with discontinuous approximations is new and our main objective was to see whether that can help to reduce the computational costs, and to improve the accuracy of the numerical solution. Since this work is preliminary to a study on Helmholtz equations, we have chosen to use an IPDGM which is well-known to be stable and consistent for wave problems [16]. Our main results are the following:

Concerning the asymptotic cost of the upscaling algorithm, it is of order $(N^2M^6+N^6)\gamma_p^3$ (γ_p denotes the number of degree of freedom per cell), while it is of order $N^6\gamma_p^3$ on the coarse mesh, and $N^6M^6\gamma_p^3$ on the fine mesh without upscaling.

Regarding numerical experiments with $\mathbb{Q}_1$ elements, we have observed a second order convergence for both IPDGM and FEM when the coarse mesh is refined whereas a zero order convergence holds for both IPDGM and FEM when the fine mesh is refined only. Operator-based uspcaling improves the accuracy of the solution for both approximations. The improvement is more significant for IPDGMs than for FEMs, knowing that IPDGMs perform better than FEMs without upscaling. Since discontinuous approximations are known to be cheaper when using higher order elements, a future work should focus on the combination of operator-based uspcaling with a high order IPDGM and obviously on extending this work to the Helmholtz equation.

References

[1] M. Christie, Upscaling for reservoir simulation, J. Petrol. Tech. 48 (1996) 1004–1010.
[2] P. King, J. Williams, Upscaling permeability: mathematics of renormalization, Transp. Porous Media 23 (1996) 337–354.
[3] G. Allaire, Homogenization and two-scale convergence, SIAM J. Math. Anal. 23 (6) (1992) 1482–1518.
[4] A. Bensoussan, J.-L. Lions, G. Papanicolaou, Asymptotic Analysis for Periodic Structures, in: Studies in Mathematics and its Applications, vol. 5, North-Holland Publishing Co., Amsterdam, 1978.
[5] J.-L. Lions, Some methods in the mathematical analysis of systems and their control, in: Kexue Chubanshe, Science Press, Beijing, 1981.
[6] T. Arbogast, S. Minkoff, P. Keenan, An operator-based approach to upscaling the pressure equation, Comput. Methods Water Resour. XII (1998) 405–412.

[7] T. Arbogast, Analysis of a two-scale, locally conservative subgrid upscaling for elliptic problems, SIAM J. Numer. Anal. 42 (2) (2004) 576–598 (electronic).
[8] T. Vdovina, S. Minkoff, An a priori error analaysis of operator upscaling for the wave equation, Int. J. Numer. Anal. Model. 5 (2008) 543–569.
[9] O. Korostyshevskaya, S. Minkoff, A matrix analysis of operator-based upscaling for the wave equation, SIAM J. Numer. Anal. 44 (2006) 586–612.
[10] T. Vdovina, S. Minkoff, S. Griffith, A two-scale solution algorithm for the elastic wave equation, SIAM J. Sci. Comput. 31 (2009) 3356–3386.
[11] D.N. Arnold, F. Brezzi, B. Cockburn, L.D. Marini, Unified analysis of discontinuous Galerkin methods for elliptic problems, SIAM J. Numer. Anal. 39 (2002) 1749–1779.
[12] D.N. Arnold, An interior penalty finite element method with discontinuous elements, SIAM J. Numer. Anal. 19 (4) (1982) 742–760.
[13] F. Bassi, S. Rebay, A high-order accurate discontinuous finite element method for the numerical solution of the compressible Navier–Stokes equations, J. Comput. Phys. 131 (1997) 267–279.
[14] C. Agut, J. Diaz, Stability analysis of the interior penalty discontinuous Galerkin method for the wave equation, INRIA Research Report, 2010.
[15] S. Prudhomme, F. Pascal, J.T. Oden, A. Romkes, Review of a priori error estimation for discontinuous Galerkin methods, TICAM REPORT 00-27, Texas Institute for Computational and Applied Mathematics, The University of Texas at Austin, 2000.
[16] M.J. Grote, D. Schötzau, Optimal error estimates for the fully discrete interior penalty DG method for the wave equation, J. Sci. Comput. 40 (2009) 257–272. http://dx.doi.org/10.1007/s10915-008-9247-z.